NJC

ROYAL SOCIETY OF CHEMISTRY

COMMUNICATION

View Article Online
View Journal | View Issue

Cite this: *New J. Chem.*, 2025, **49**, 18244

Received 29th July 2025,
Accepted 21st September 2025

DOI: 10.1039/d5nj03066h

rsc.li/njc

Linear and looped coordination polymers of hemoglobins linked *via* bis(terpyridine)iron(II) complexes

Yoshitsugu Morita, Remi Sawaguchi, Taiga Yamada and Teruyuki Komatsu *

We synthesized two structurally distinct coordination polymers of hemoglobins (Hbs) linked *via* bis(terpyridine)iron(II) complexes. Modulating the angle between the two terpyridine ligands on Hb yielded either linear nanofibers or looped nanofibers with discrete nanorings. These Hb-based polymers retained the intrinsic O_2-binding capacity of the native Hb units under physiological conditions.

Coordination polymers formed through iterative metal–ligand assembly between multidentate ligands and metal ions have garnered significant attention in materials chemistry owing to their structural diversity and emergent functionalities.[1,2] In particular, bis(terpyridine) ligands exhibit high-affinity, selective coordination with divalent metal ions, such as iron(II), cobalt(II), zinc(II), and ruthenium(II), making them indispensable motifs for engineering various metal–organic architectures.[3–8] Proteins, as nature's most intricate macromolecular systems, underpin fundamental biological processes. Advances in protein engineering and chemical modification have enabled their transformation into programmable building blocks for constructing functional coordination assemblies.[9–11] Notable examples include streptavidin derivatives equipped with bis(terpyridine) moieties that form one-dimensional bundles upon iron(II) coordination, as reported by Ward *et al.*,[12] and His-tagged glutathione S-transferase forming a nanoring with nickel(II), demonstrated by Liu *et al.*[13] Hayashi and co-workers synthesized supramolecular trimers of cytochrome b_{562} and examined their thermodynamic stability.[14] Despite these developments, the majority of studies have emphasized morphological outcomes, with relatively limited insight into the resulting structure–function relationships. Recently, Tezcan *et al.* designed two-dimensional protein crystals whose conformation dynamically responds to cobalt(II) coordination, undergoing reversible opening upon exposure to hydrogen cyanide.[15] In our previous work, we demonstrated that the ubiquitous blood protein human serum albumin (HSA) can serve as a scaffold for fiber formation, yielding nanostructures that exhibit enzyme-like activity under aqueous environments.[16] Building upon this strategy, we now report the synthesis of coordination polymers composed of the prototypical heme protein hemoglobins (Hbs), linked *via* bis(terpyridine)iron(II) complexes. Remarkably, the geometric configuration of the resulting nanofibers—either linear or looped—was governed by the relative angle between the two terpyridine units introduced onto each Hb molecule. Crucially, all polymers retained the native O_2-binding capacity of their monomeric Hb components, indicating successful preservation of both structural integrity and biological function.

To systematically control the inter-ligand angle between the two terpyridine moieties (180, 120, or 90°), we designed three Hb variants bearing two strategically positioned reactive Cys residues (Fig. 1). The 180° variant, designated rHb120, is a recombinant αα-fused (Arg-$\alpha_1$141–Val-$\alpha_2$1) (di-α bridged) Hb in which the Lys-β120 residues at symmetric positions were replaced with Cys, while the native Cys-β93 was substituted with Ala to eliminate undesired reactivity. The 120° variant, rHb17, is another di-α recombinant construct in which Lys-β17 is substituted with Cys and Cys-β93 with Ala. Both rHb120 and rHb17 were heterologously expressed in *Pichia pastoris* following our established protocols.[16,17] The 90° variant, designated XHb, was generated *via* chemical crosslinking of two Lys-β82 residues using bis(3,5-dibromosalicyl)fumarate (DBBF), while preserving the two native Cys residues in their reactive thiol state. SDS-PAGE analysis confirmed the structural modifications: the α-subunit band was absent in both rHb120 and rHb17, while the β-subunit band was absent in XHb (Fig. S1), consistent with successful intramolecular crosslinking. Quantitative thiol analysis using 4,4′-dithiodipyridine[18] revealed that each Hb variant retained two reactive Cys residues per molecule, validating the design and availability of conjugation sites.

Subsequently, the maleimide-functionalized terpyridine derivative, 4′-{2‴-[4⁗-(*N*-maleimidomethyl)cyclohexanoylamino]-ethoxy}-2,2′:6′,2″-terpyridine (Mal-Tpy), was conjugated to rHb17

Department of Applied Chemistry, Faculty of Science and Engineering, Chuo University, 1-13-27 Kasuga, Bunkyo-ku, Tokyo 112-8551, Japan.
E-mail: komatsu@kc.chuo-u.ac.jp

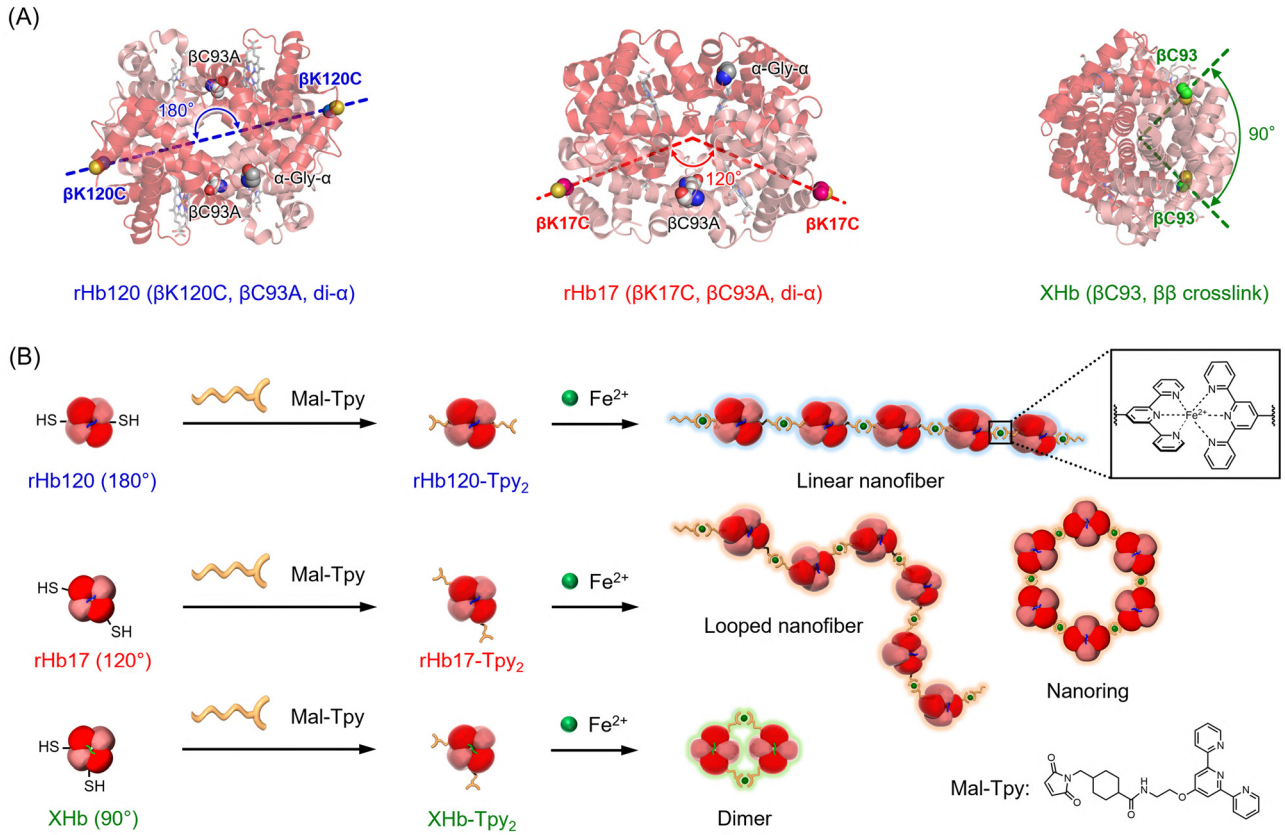

Fig. 1 (A) Positions of Cys residues on rHb120, rHb17, and XHb. (B) Synthesis scheme of coordination polymers of Hb: linear nanofiber, looped-nanofiber with nanoring, and dimer.

to yield the bis(terpyridine)-modified Hb, rHb17-Typ$_2$ (Fig. 1B). Sulfhydryl quantification revealed a 0% remaining free thiol content, confirming complete modification of the two Cys-β17 residues. Additionally, the UV-vis absorption spectrum of rHb17-Tpy$_2$ corresponded closely with the theoretical sum of the spectra of rHb17 and twice that of Mal-Tpy (Fig. S2), further supporting successful dual-site conjugation. Analogous modifications were performed on rHb120 and XHb using Mal-Tpy to afford rHb120-Tpy$_2$ and XHb-Tpy$_2$, respectively (Fig. 1B).

Upon stepwise addition of $FeCl_2{\cdot}4H_2O$ to an aqueous solution of rHb17-Tpy$_2$, a proportional increase in UV-vis absorbance was observed as a function of the Fe(II)/rHb17-Tpy$_2$ ratio, indicative of the formation of bis(terpyridine)iron(II) [Tpy$_2$-Fe(II)] complexes (Fig. 2A). In related nanofiber coordination polymers based on HSA bearing two terpyridine arms, the Tpy$_2$-Fe(II) complex exhibits metal-to-ligand charge transfer (MLCT) absorption at 557 nm and an intraligand $\pi \rightarrow \pi^*$ transition at 315 nm.[5,7,16,19] However, in the case of Hb, strong Q-bands arising from the heme prosthetic groups overlap in the 500–600 nm region, complicating direct observation of the MLCT transition. To circumvent this interference, we monitored complex formation *via* the increase in absorption at 315 nm. Saturation of the spectral change at an equimolar ratio indicated the stoichiometric formation of a 1 : 1 complex between rHb17-Tpy$_2$ and iron(II) (Fig. 2B). Equivalent titration experiments with rHb120-Tpy$_2$ and XHb-Tpy$_2$ yielded comparable results (Fig. 2B, Fig. S3).

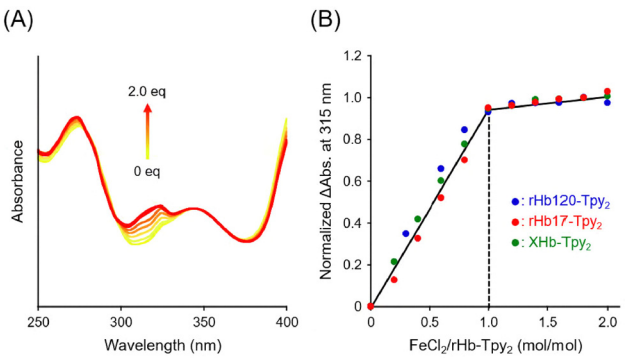

Fig. 2 (A) UV-vis absorption spectral changes of aqueous rHb17-Tpy$_2$ solution (5 μM) upon addition of $FeCl_2$ at 25 °C. (B) Absorbance increase (ΔAbs. at 315 nm) of aqueous rHb120-Tpy$_2$, rHb17-Tpy$_2$, and XHb-Tpy$_2$ solution (5 μM) upon addition of $FeCl_2$ at 25 °C.

Transmission electron microscopy (TEM) images of uranyl acetate-stained [(rHb120-Tpy$_2$)-Fe(II)]$_n$ assemblies revealed elongated, linear nanofibers with a uniform width of approximately 4 nm (Fig. 3A). Given that the native diameter of Hb is approximately 6 nm,[20] the observed fiber width appeared narrower than expected. This discrepancy likely arises from the loose, low-density packing of globular Hb units within the polymer, which may reduce staining contrast and yield an underestimation of the apparent fiber dimensions. The nanofibers typically extended to

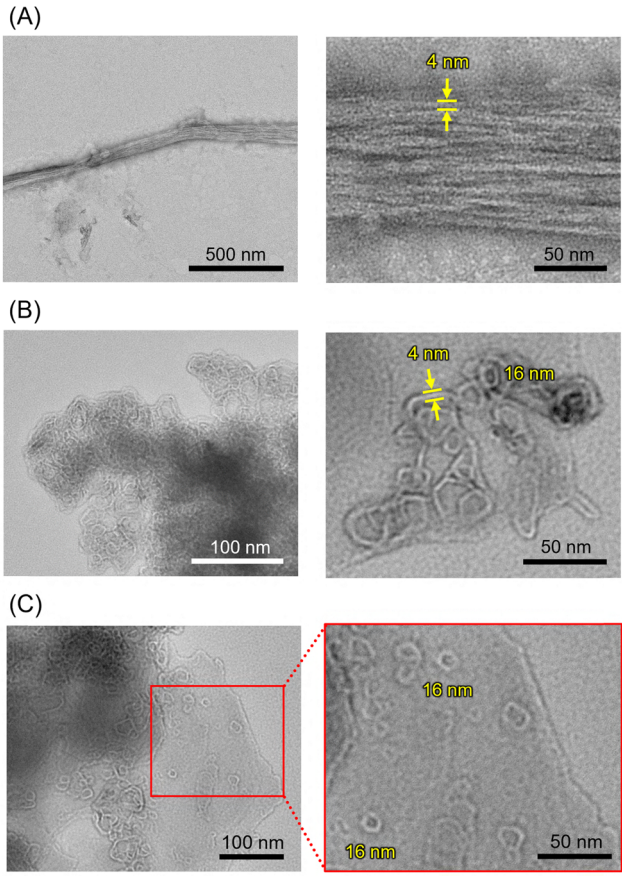

Fig. 3 TEM images of (A) linear [rHb120-Tpy$_2$-Fe(II)]$_n$ nanofibres, (B) looped [rHb17-Tpy$_2$-Fe(II)]$_n$ nanofibers with nanorings, and (C) an isolated fraction of [rHb17-Tpy$_2$-Fe(II)]$_n$ nanorings.

lengths of ~1 μm, suggesting that each polymer chain consists of ~160 Hb monomers. Moreover, the nanofibers exhibited a tendency to bundle into extended aggregates exceeding 2 μm in length (Fig. 3A), consistent with previously reported Hb-based fibers lacking di-α linkage.[16] These observations support the conclusion that rHb120-Tpy$_2$, with its two terpyridine arms oriented at 180°, undergoes linear coordination polymerization *via* iron(II) bridging, resulting in well-ordered straight nanofibers.

In stark contrast, TEM imaging of [(rHb17-Tpy$_2$)-Fe(II)]$_n$ revealed the formation of structurally distinct looped nanofibers (Fig. 3B). The fibers maintained a consistent width of 4 nm, again narrower than the native Hb diameter, likely due to similar packing effects. Notably, altering the angular orientation of the terpyridyl groups from 180° (rHb120-Tpy$_2$) to 120° (rHb17-Tpy$_2$) significantly disrupted linearity, giving rise to curved, loop-like architectures. Intriguingly, discrete nanorings with diameters of approximately 16 nm were clearly observed, indicating the formation of closed macrocyclic structures with the polymer matrix.

Conversely, the [(XHb-Tpy$_2$)-Fe(II)]$_n$ complex, in which the two terpyridine moieties are oriented at a 90° angle, did not yield any observable nanostructures. No fibers were detected in the TEM images. We postulate that coordination of two XHb-Tpy$_2$ units with iron(II) leads to the formation of a non-propagating dimer, precluding further polymerization and thereby preventing fiber assembly.

Among the supramolecular assemblies, particular attention was directed toward the [(rHb17-Tpy$_2$)-Fe(II)]$_n$ nanorings, with the aim of isolating and characterizing their structure and properties. Size exclusion chromatography (SEC) was employed to analyze the Hb nanorings. As a control experiment, an aqueous solution of the [(rHb120-Tpy$_2$)-Fe(II)]$_n$ complex—which forms linear nanofibers—was passed through a sterilizing membrane filter (pore size: 0.2 μm) to remove long fibers prior to SEC analysis. Although the majority of the polymeric species were excluded by filtration, the SEC profile of the filtrate displayed seven distinct peaks corresponding to low-molecular-weight oligomers (Fig. 4A). These oligomeric species, including the rHb120-Tpy$_2$ monomer, likely arose from partial dissociation of the bis(terpyridine)iron(II) complexes due to dilution during SEC analysis. The primary peak ($n > 7$) appeared near the exclusion limit of the SEC column. The elution times of the remaining six peaks showed a linear correlation with the molecular weights of (rHb120-Tpy$_2$)-based oligomers ranging from monomer ($n = 1$) to hexamer ($n = 6$) (Fig. 4B). Under dilute conditions, native Hb typically dissociates from its $\alpha_2\beta_2$ tetrameric form into αβ dimers. However, in the rHb120 construct, the engineered di-α linkage effectively stabilized the αβ interfaces, thereby preventing such dissociation. As a result, the [(rHb120-Tpy$_2$)-Fe(II)]$_n$ complexes retained their fibrous architectures even at low concentrations.

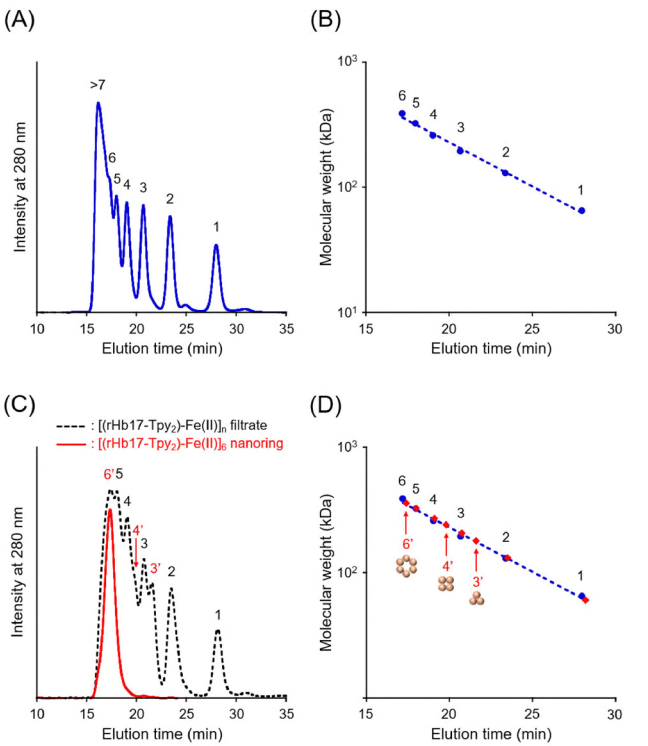

Fig. 4 (A) SEC profile and (B) relationship between elution time and molecular weight of [(rHb120-Tpy$_2$)-Fe(II)]$_n$ oligomers using a Superdex 200 increase 10/300 GL column (Cytiva). (C) SEC profile and (D) relationship between elution time and molecular weight of [(rHb17-Tpy$_2$)-Fe(II)]$_n$ oligomers using a Superdex 200 increase 10/300 GL column (Cytiva).

Following an analogous procedure, the filtered solution of the looped $[(rHb17\text{-}Tpy_2)\text{-}Fe(II)]_n$ assemblies containing nanorings was subjected to SEC. The resulting elution profile exhibited multiple peaks (Fig. 4C), with peaks 1–5 matching those observed for the $[(rHb120\text{-}Tpy_2)\text{-}Fe(II)]_n$ control (Fig. 4D). Notably, detailed analysis revealed that the elution times of peaks 3′, 4′, and 6′ were delayed relative to their linear counterparts (peaks 3, 4, and 6), indicating reduced hydrodynamic volumes. In general, ring-shaped structures exhibit smaller effective molecular dimensions than their linear analogues of equivalent molecular weight, resulting in slower elution. We therefore attributed peaks 3′, 4′, and 6′ to annular trimeric, tetrameric, and hexameric species, respectively. The 120° inter-ligand angle of rHb17-Tpy_2 appears to favor the formation of closed-loop topologies, particularly hexameric nanorings, *via* iron(II)-mediated coordination. Preparative SEC using a Superdex 200 Increase (Cytiva) enabled the isolation of the hexameric $[(rHb17\text{-}Tpy_2)\text{-}Fe(II)]_6$ nanoring fraction (Fig. 4C). Dynamic light scattering (DLS) measurements of the collected fraction revealed a hydrodynamic diameter of 13.5 ± 7.5 nm, significantly larger than that of the rHb17-Tpy_2 monomer (6.2 ± 3.5 nm). The low polydispersity index (PDI = 0.023) further supported the selective formation of uniform nanorings. However, TEM imaging of the isolated fraction revealed the presence of both nanorings and looped fibers (Fig. 3C), suggesting that the closed-ring conformation is entropically unstable and susceptible to conversion into extended polymeric forms. Indeed, the SEC peak of the $[(rHb17\text{-}Tpy_2)\text{-}Fe(II)]_6$ nanoring gradually diminished over 24 h at 4 °C, consistent with a thermodynamic equilibrium between the ring and the fiber states. Due to this dynamic instability, it was not possible to further characterize the isolated Hb nanorings in their pure form.

Finally, the O_2-binding properties of the Hb-based assemblies were systematically evaluated. UV-vis absorption spectra of the linear $[(rHb120\text{-}Tpy_2)\text{-}Fe(II)]_n$ nanofibers, looped $[(rHb17\text{-}Tpy_2)\text{-}Fe(II)]_n$ nanofibers with nanorings, and $[(XHb\text{-}Tpy_2)\text{-}Fe(II)]_2$ dimers in phosphate-buffered saline (PBS) solutions (pH 7.4) under an N_2 atmosphere were virtually identical to that of native deoxy-Hb (Fig. S4). Upon exposure to O_2 gas, all spectra underwent a rapid and characteristic transition to the oxy form. Furthermore, stable carboxy complexes were readily formed upon CO gas treatment. The maximum absorption wavelengths of the deoxy, oxy, and carboxy forms of the Hb polymers were nearly identical to those of native Hb and the corresponding monomeric precursors (rHb120, rHb17, and XHb) (Table S1). Interestingly, the Soret band intensity of the deoxy form of the Hb nanofibers was slightly diminished relative to that of native Hb (Fig. S4). The quaternary structure of Hb is known to undergo a conformational shift from a low-affinity tense (T) state to a high-affinity relaxed (R) state upon oxygenation. Perutz *et al.* reported that an unusual deoxy-R conformation exhibits a notably reduced Soret band absorbance compared to the canonical T state.[21] The Hb subunits embedded within the nanofibers and nanorings likely adopt a conformation biased toward the R state, impeding their ability to fully revert to the T-state structure in the absence of O_2.

To further investigate the effects of protein engineering and polymerization on O_2 affinity, we determined O_2-binding equilibrium parameters—P_{50} (the partial pressure of O_2 at which Hb is 50% saturated) and the Hill coefficient n (reflecting cooperativity in O_2 binding)—from O_2 dissociation curves (Fig. S5). The rHb precursors (rHb120, rHb17, and XHb) exhibited P_{50} values of 9–11 Torr and Hill coefficients of 1.3–1.9 at 37 °C (Table 1), indicating slightly higher O_2 affinity and reduced cooperativity compared to native Hb. These differences are consistent with previous reports, demonstrating that (i) covalent intramolecular bridging restricts Hb's quaternary structural transition,[22] and (ii) chemical modification of Cys-β93, located adjacent to the proximal His-β92, enhances O_2 affinity while reducing cooperativity.[23–26] We hypothesized that cooperative allosteric communication might propagate across adjacent subunits upon O_2 binding, potentially amplifying cooperative behavior. However, O_2-binding analysis of the linear $[(rHb120\text{-}Tpy_2)\text{-}Fe(II)]_n$ nanofibers, the looped $[(rHb17\text{-}Tpy_2)\text{-}Fe(II)]_n$ nanofibers with nanorings, and the $[(XHb\text{-}Tpy_2)\text{-}Fe(II)]_2$ dimers all yielded P_{50} values in the range of 8–12 Torr and Hill coefficients of 1.3–1.4—essentially indistinguishable from their respective monomeric precursors. These results clearly demonstrate that the polymerization of Hb through bis(terpyridine)iron(II) coordination preserves the intrinsic O_2-binding properties of each Hb unit without inducing cooperative enhancement. Conversely, this finding suggests that O_2-binding parameters such as P_{50} can be systematically tuned by introducing site-specific mutations in the heme environment, independent of the polymeric framework.

Table 1 O_2-binding parameters of Hb nanofibers and Hb precursors in PBS solution (pH 7.4, 37 °C)

Hemoproteins	P_{50} (Torr)	n (—)
Hb	12	2.4
rHb120	11	1.3
$[(rHb120\text{-}Tpy_2)\text{-}Fe(II)]_n$ nanofiber	12	1.3
rHb17	10	1.3
$[(rHb17\text{-}Tpy_2)\text{-}Fe(II)]_n$ nanofiber with nanoring	12	1.3
XHb	9	1.9
$[(XHb\text{-}Tpy_2)\text{-}Fe(II)]_2$ dimer	8	1.4

Conclusions

We successfully demonstrated the formation of two distinct coordination polymer architectures of blood protein Hb through complexation of its bis(terpyridine) moieties with iron(II) ions. By modulating the relative angular orientation of the two terpyridine ligands on Hb from 180° to 120°, the resulting supramolecular assemblies transitioned from linear nanofibers to looped nanofibers incorporating discrete nanorings. Notably, these coordination polymers preserved the inherent, reversible O_2-binding capacity of the Hb units. This work introduces a novel strategy for constructing functional hybrid materials that integrate metallosupramolecular motifs with biologically active protein scaffolds, offering new insights into structure–function relationships at the interface of coordination chemistry and protein engineering.

Author contributions

T. K. designed and initiated this study. All the authors conducted experiments and analyzed the data. R. S., T. Y. and T. K. drafted the manuscript.

Conflicts of interest

There are no conflicts to declare.

Data availability

The data supporting this article have been included as part of the supplementary information (SI). Supplementary information: experimental section, SDS-PAGE analysis of rHb120, rHb17, and XHb, UV-vis absorption spectra of rHb17-Tpy_2, UV-vis absorption spectral changes upon addition of $FeCl_2$ in rHb120-Tpy_2 and XHb-Tpy_2 solution, and UV-vis absorption spectra, data, and O_2 dissociation curves of Hb fibers and Hb precursors. See DOI: **https://doi.org/10.1039/d5nj03066h**.

Acknowledgements

This work was supported by JSPS KAKENHI Grant Numbers JK24K01302 and JK25K22923.

References

1 H. Nishihara, *Chem. Lett.*, 2014, **43**, 388.
2 J. Zhao, J. Yuan, Z. Fang, S. Huang, Z. Chen, F. Qiu, C. Lu, J. Zhu and X. Zhuang, *Coord. Chem. Rev.*, 2022, **471**, 214735.
3 E. C. Constable and A. M. W. C. Thompson, *J. Chem. Soc., Dalton Trans.*, 1992, 3467.
4 C. Wei, Y. He, X. Shi and Z. Song, *Coord. Chem. Rev.*, 2019, **385**, 1.
5 Y. Wang, T. Liu, L. Chen and D. Chao, *Inorg. Chem.*, 2021, **60**, 5590.
6 P. Verma, A. Singh, F. A. Rahimi, P. Sarkar, S. Nath, S. K. Pati and T. K. Maji, *Nat. Commun.*, 2021, **12**, 7313.
7 M. T. Gamache, B. Gehring, G. S. Hanan and D. G. Kurth, *Dalton Trans.*, 2024, **53**, 13151.
8 M. K. Bera, S. Sarmah, D. C. Santra and M. Higuchi, *Coord. Chem. Rev.*, 2024, **501**, 215573.
9 Q. Luo, C. Hou, Y. Bai, R. Wang and J. Liu, *Chem. Rev.*, 2016, **116**, 13571.
10 J. Zhu, N. Avakyan, A. Kakkis, A. M. Hoffnagle, K. Han, Y. Li, Z. Zhang, T. S. Choi, Y. Na, C. J. Yu and F. A. Tezcan, *Chem. Rev.*, 2021, **121**, 13701.
11 R. Liu, L. Li, S. Chen, Z. Yang, Z. Kochovski, S. Mei, Y. Lu, L. Zhang and G. Chen, *ACS Nano*, 2023, **17**, 2245.
12 S. Burazerovic, J. Gradinaru, J. Pierron and T. R. Ward, *Angew. Chem., Int. Ed.*, 2007, **46**, 5510.
13 Y. Bai, Q. Luo, W. Zhang, L. Miao, J. Xu, H. Li and J. Liu, *J. Am. Chem. Soc.*, 2013, **135**, 10966.
14 K. Oohora, R. Kajihara, N. Fujimaki, T. Uchihashi and T. Hayashi, *Chem. Commun.*, 2019, **55**, 1544.
15 S. Vijayakumar, R. G. Alberstein, Z. Zhang, Y. S. Lu, A. Chan, C. E. Wahl, J. S. Ha, D. E. Hunka, G. R. Boss, M. J. Sailor and F. A. Tezcan, *Nat. Commun.*, 2024, **15**, 6326.
16 R. Adachi, S. Suzuki, T. Mitsuda, Y. Morita and T. Komatsu, *Chem. Commun.*, 2020, **56**, 15585.
17 Y. Morita, Y. Shindo and T. Komatsu, *Chem. Lett.*, 2021, **50**, 2011.
18 D. R. Grassetti and J. F. Murry Jr., *Arch. Biochem. Biophys.*, 1967, **119**, 41.
19 P. S. Braterman, J.-I. Song and R. D. Peacock, *Inorg. Chem.*, 1992, **31**, 555.
20 R. Funaki, W. Okamoto, C. Endo, Y. Morita, K. Kihira and T. Komatsu, *J. Mater. Chem. B*, 2020, **8**, 1139.
21 M. F. Perutz, J. E. Ladner, S. R. Simon and H. Chien, *Biochemistry*, 1974, **13**, 2163.
22 T. Yamada, M. Katsumi, K. Ishii and T. Komatsu, *Chem. – Asian J.*, 2024, **19**, e202400257.
23 D. Li, T. Hu, B. N. Manjula and S. A. Acharya, *Bioconjugate Chem.*, 2009, **20**, 2062.
24 T. J. Styslinger, N. Zhang, V. S. Bhatt, N. Pettit and A. F. Palmer, *J. Am. Chem. Soc.*, 2012, **134**, 7507.
25 Y. Morita, T. Yamada, M. Kureishi, K. Kihira and T. Komatsu, *J. Phys. Chem. B*, 2018, **122**, 12031.
26 N. Kohyama, T. Takamine, W. Okamoto, T. Yamada, M. Yamaguchi, M. Kohno, R. Tochinai and T. Komatsu, *ACS Appl. Bio Mater.*, 2025, **8**, 2397.

